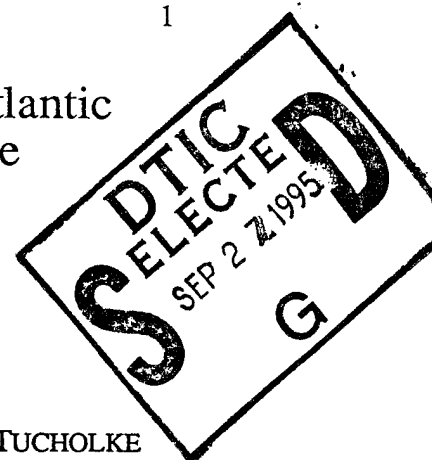# Quantitative Analysis of Abyssal Hills in the Atlantic Ocean: A Correlation Between Axis Mantle Temperature and Extensional Faulting

JOHN A. GOFF

University of Texas Institute for Geophysics, Austin, Texas

JIAN LIN, GARY E. JAROSLOW, MARTIN C. KLEINROCK, AND BRIAN E. TUCHOLKE

Woods Hole Oceanographic Institution, Woods Hole, Massachusetts

A recent cruise to the ONR Atlantic Natural Lab gathered 100% Hydrosweep bathymetric coverage, >200% MR1 side-scan coverage, gravity and magnetics over an area spanning three ridge segments along axis (~25°25'N to ~27°10'N) and crustal ages from 0 to 30 Ma west of the Mid-Atlantic Ridge. This data set represents a first opportunity for an extensive regional analysis of abyssal created at a slow spreading rate ridge. We apply the method of Goff and Jordan (1988) for the estimation of 2-D statistical properties of abyssal hill morphology from the gridded Hydrosweep bathymetry. Important abyssal hill parameters derived from this analysis include the rms height, characteristic width, plan-view aspect ratio, and lineament azimuth. The primary purpose of this work is to further constrain the relationship between abyssal hill morphology and the properties of the ridge crest at which they were formed. The analysis is segmented into two sub-studies: analysis of near axis (< 7 Ma) abyssal hills for each of the three segments, and analysis of temporal variations (~1-29 Ma) in abyssal hill morphology along the southern segment (the only segment that clearly persists over the entire age range sampled). The results of this analysis are compared and correlated with analysis of the gravity data and the determination of faulting characeristics based on the MR1 side-scan data. Principal results include: (1) Abyssal hill morphology within the study region is strongly influenced by the inside/outside corner geometry of the mid-ocean ridge segments; inside corners produce abyssal hills with larger rms height and characteristic width and smaller plan-view aspect ratios than abyssal hills produced at outside corners. (2) Along the southern segment flow line, lineament azimuths, where not affected by evident propagator structures or inside corners, are generally perpendicular to the anticipated flow line????????>>>>need mag anom trends<<<<(3) Both the inter-segment and flow-line variation in rms height and, to a lesser extent, characteristic width of abyssal hills are positively correlated with residual gravity anomaly. This implies that smaller abyssal hills are produced when the crust being generated is thicker (i.e., when the mantle beneath the axis is hotter) and larger abyssal are produced when the crust being generated is thinner (i.e., when the mantle beneath the axis is colder). (4) Variations in average near-axis rms heights over the three segments negatively correspond with variations in average faulting density as determined from analysis of MR1 side-scan imagery. This is circumstantial evidence supporting the assertion that faulting plays a dominant role in abyssal hill formation at slow spreading rates.

INTRODUCTION

The process of abyssal hill formation at mid-ocean ridge crests is one of the least-understood components of the ridge system. Abyssal hills are highly statistical in nature, and as such present a unique set of challenges both for quantitative characterization and for physical modeling of the processes that create them. Quantitative characterization of abyssal hill morphology has received much attention in recent years [e.g., *Krause and*

Menard, 1965; *Menard and Mammerickx*, 1967; *McDonald and Katz*, 1969; *Bell*, 1975, 1978; *Fox and Hayes*, 1985; *Gilbert and Malinverno*, 1988; *Goff and Jordan*, 1988; *Malinverno and Pockalny*, 1990; *Goff*, 1991, 1992; *Malinverno*, 1991; *Hayes and Kane*, 1991; *Goff et al.*, 1993], but few studies have yet attempted to formulate physical models of abyssal hill formation which satisfy quantitative observational constraints [*Schouten and Denham*, 1983; *Malinverno and Gilbert* 1989; *Malinverno and Cowie*, 1993]. It can be argued, however, that this is a necessary sequence to solving this problem. Physical models are tested by how well they match observations. Hence, before physical models can be generated, one must know the manner in which observations will be made and the quantitative parameters which distinguish one terrain from another.

This paper continues the work of quantitative characterization of abyssal hill morphology. Previous contributions to this effort have included studies relating abyssal hill morphology to spreading rate variations [*Menard*, 1967; *Malinverno*, 1991; *Hayes and Kane*; 1991; *Goff*, 1991, 1992] and studies relating abyssal hill morphology to ridge segmentation at fast spreading rates [*Goff*, 1991; *Goff et al.* 1993]. This study seeks to expand on this work by relating abyssal hill morphology to ridge segmentation and temporal variability at slow spreading rates. Our principal data set consists of Hydrosweep swath bathymetry [*Chayes et al.*, 1991] collected on a recent geophysical reconnaissance of the ONR Acoustic Reverberation Corridor [*Tucholke et al.*, 1990] aboard the *R/V Maurice Ewing*. This cruise succeeded in obtaining nearly 100% Hydrosweep bathymetric coverage as well as gravity, magnetic, and >200% HMR1 side scan [*Rognstad*, 1992] coverage in a region extending from near the Mid-Atlantic Ridge (MAR) axis westward out to ~30 Ma crust, and covering three ridge segments from ~25°25'N to ~27°10'N (Figures 1 and 2).

The work presented here utilizes the methodology of *Goff and Jordan* [1988, 1989] and *Goff* [1990] for the estimation of statistical parameters through formalized inversion of bathymetric data. These parameters include the second order statistical parameters rms height, characteristic width and length, plan-view aspect ratio, lineament azimuth and fractal dimension as well as the higher-order (i.e., non-Gaussian) parameters skewness, tilt, and kurtosis (peakiness).

Quantitative analysis of abyssal hill morphology has begun to place observational constraints on the process of generation of seafloor and crust at mid-ocean ridge systems. Several studies have attempted to correlate abyssal hill characteristics with spreading rate [*Menard*, 1967; *Malinverno*, 1991; *Hayes and Kane*; 1991; *Goff*, 1991, 1992], and most of these have focused on abyssal hill rms height. These studies are all consistent in the observation that rms heights are generally larger at slower spreading rates. The

relationship between rms height and spreading rate is not strictly linear, exhibiting a steep negative correlation up to approximately 60 mm/yr half rate, and little apparent correlation at higher spreading rates (though both *Goff* [1991] and *Malinverno* [1991] noted a possible slight positive correlation between rms height and spreading rates above 60 mm/yr half rate).

The negative correlation of abyssal hill rms height with spreading rate can probably be attributed, at least in part, to the effect of variation in thermal structure on the process of abyssal hill faulting. The crust and lithosphere in the vicinity of slow spreading ridge axes is cooler relative to fast spreading ridges [*Phipps-Morgan et al.*, 1987; *Chen and Morgan*, 1990], allowing for greater elastic thickness [*McNutt*, 1984]. Near-axis faults can therefore extend deeper and a greater fault throw can accommodate crustal extension before another fault must be created [*Forsyth*, 1992]. In addition, the cooler thermal structure at slow spreading ridges results in necking of the lithosphere (creation of the rift valley) [*Tapponnier and Francheteau*, 1978; *Phipps-Morgan et al.*, 1987; *Lin and Parmentier*, 1989; *Chen and Morgan*, 1990] which is very rarely observed at fast spreading rates [e.g., *Macdonald*, 1982]. Formation of a rift valley is accommodated by large displacements on inward-facing faults which are preserved off-axis as abyssal hill-forming structures. Also, the difference in style of primary extruded volcanics (edifice formation at slow spreading ridges versus sheet flows at fast spreading ridges) [*CYAMEX*, 1981] favors the formation of taller volcanic edifices at slow spreading ridges than at fast spreading ridges.

The variation of rms height with spreading rate is, however, only one small part of the relationship between abyssal hills and the ridge system at which they were formed. For example, *Goff* [1991] found that abyssal hills formed at the East Pacific Rise (fast spreading) possess fundamentally different shape and texture characteristics than those produced along the Mid-Atlantic Ridge (slow spreading). Differences are manifest in a variety of statistical measures, including characteristic width and length, the correlation between rms height and characteristic width, plan-view aspect ratio, correlation between rms height and aspect ratio, skewness, tilt, and kurtosis; texturally, MAR abyssal hills are of an entirely different species than East Pacific Rise (EPR) abyssal hills. This observation leads to inference that the tectonic and/or volcanic processes involved in the process of abyssal hill formation are fundamentally different for the two spreading ridges (though precisely what those difference are remains to be determined).

Despite the association of much of the variation in abyssal hill characteristics to variation in spreading rate (or at least identification of EPR and MAR types of abyssal hills), a significant amount of abyssal hill character variation occurs on a regional scale,

not attributable to spreading rate variation. Studies by *Goff* [1991] and *Goff et al.* [1993] on multibeam data sets along the flanks of the EPR show that much of this additional variation can be attributed to the segmentation of the mid-ocean ridge crest. In particular, rms height (the most well-resolved statistical parameter) tends to be largest toward the ends of segments (bounded by first- or second-order discontinuities) and smallest toward the middle. The rms height of abyssal hills adjacent to the EPR is predominantly fault controlled [*Lonsdale*, 1977; *Bicknell et al.*, 1987], and segmentation of the ridge crest (to first- and second-order discontinuities) is largely attributable to variations in mantle upwelling (more robust upwelling toward the segment middle) [*Macdonald and Fox*, 1988; *Cochran et al.*, 1993]. Hence, as with rms height variations associated with spreading rate, rms height variations associated with segmentation may be attributed to the relationship between extensional faulting and the thermal structure of the lithosphere in the vicinity of the ridge axis.

Characteristic widths of abyssal hills in the EPR region 9°N-16°N are negatively correlated with rms heights [*Goff*, 1991], and in the EPR region 7°S-9°S there is no correlation between these parameters. This is perhaps a counterintuitive result, as we might expect abyssal hills to be wider if they are taller. There is at present no obvious explanation for this observation.

Because of the great differences between MAR- and EPR-created abyssal hills, we cannot expect the results of the EPR regional studies [*Goff*, 1991; *Goff et al.*, 1993] to be similar to the results of this regional analysis of MAR abyssal hills. In fact the results presented here do display marked differences. For example, in this study rms heights and characteristic widths are found to vary drastically between adjacent segments, something not seen in EPR abyssal hills. Also, the variation in rms heights within each MAR segment is dominated by the inside/outside corner geometry rather than the upwelling pattern at the ridge axis as with EPR abyssal hills.

However, despite these differences, we do find evidence in this study, as with both the spreading-rate and regional EPR studies, that rms heights are strongly influenced by the degree of mantle upwelling or temperature structure beneath the mid-ocean ridge. In an analysis of near-axis morphology, abyssal hills within the southern of the three mapped segments have a much lower rms height than abyssal hills within the central and northern segments. This pattern is correlated with gravity analysis, which indicates that the southern ridge segment has a robust "bull's-eye" mantle bouger anomaly low, indicative of robust mantle upwelling and/or increased crustal thickness (either of which imply higher axis temperatures) while the central and northern segments do not. Also, in an analysis of abyssal hill morphology within the southern segment out to 30 Ma crustal age,

rms heights and characteristic widths are positively correlated to the residual gravity anomaly, and by inference negatively correlated with the temporal variations in crustal thickness/axis temperature within this segment.

STOCHASTIC CHARACTERIZATION

In this section we present a powerful tool for quantitative characterization of abyssal hill morphology, stochastic modeling, which we expect to enable us to continue to clarify the relationship between abyssal hills and the ridge crest at which they are formed.

The stochastic model used to characterize the second-order statistics of abyssal hill morphology and the procedure for inverting model parameters from Sea Beam data are given in detail in *Goff and Jordan* [1988; 1989] and *Goff* [1990] and summarized in *Goff* [1991; 1992]. To maintain the focus of this paper on results, discussion of the methodology is deferred to those papers. This methodology takes as input a swath of multibeam data or the gridded product and produces as output estimations of relevant physical parameters with formal uncertainties. To obtain optimal data orientation relative to segment boundaries, only gridded data were used for this analysis. Sections of the gridded data chosen for analysis consisted of elongate rectangular areas 7.5 km wide and 50-100 km long; i.e., very similar to the sampling of a single hydrosweep swath. When the long axis of the sampling box runs accross the abyssal hill grain, this data geometry is optimal for resolving statistical parameters while also resolving spatial variations in parameters along-axis.

For simplicity we refer to each elongated-box sampling of the gridded data set as a "swath" of data (this term also emphasizes similarity to multibeam sampling). Two constraints are placed on swaths chosen for input: (1) they are straight and long enough to produce well-resolved estimations [*Goff and Jordan*, 1989b], and (2) the morphology sampled does not include seamounts or segment boundaries (to the best of our ability to identify these features). Because of differences in decorrelation distances, longer data sets are required to make reasonable parameter estimations when sampling Atlantic abyssal hills than than when sampling Pacific abyssal hills. For example, whereas perhaps a 20-25 km long swath of multibeam data might be the minimum data necessary for the flanks of the EPR, perhaps a 60-75 km long swath is the minimum data necessary for the flanks of the MAR.

The output physical parameters include the following:

1. The rms height is the average variation of bathymetry about the mean depth.

2. The orientation of topography is the azimuth of the strike of abyssal hill lineaments.

3. The characteristic length is the visually dominant feature length (or wavelength) along a profile direction. It is defined by the width of the covariance along the same profile direction [*Goff and Jordan*, 1988]. Perpendicular to the grain it is called the characteristic width of abyssal hills and and parallel to the grain it is called the characteristic length.

4. The aspect ratio is the characteristic planar shape of the abyssal hills.

5. The Hausdorff (fractal) dimension is a measure of roughness. It is defined by the asymptotic properties of the covariance function as the lag $\rightarrow 0$. An increas in fractal dimension rapresents an increase in roughness, the limiting cases of 2 and 3 corresponding to a random field with continuous derivative (Euclidean surface) and one which is space filling (Peano surface) respectively.

These parameters and their uncertainties form an objective basis for morphological classification; i.e., for stating that one region is significantly different from another region and what makes them different. What these parameters cannot do at present is tell us, for example, that a certain region is dominated either by extensional tectonism or constructional volcanism. These processes are dissimilar, and it is not unreasonable to expect that the morphologies they produce will have characteristic differences which can be detected with the estimated stochastic model parameters. However, to be able to make this distinction we will need to ground-truth the statistics; i.e., match statistical characteristics with geologic characteristics. By providing information on faulting behavior, the MR1 side-scan data set that was gathered coincidentally with the Hydrosweep data should prove valuable in this regard.

In addition to the second-order statistical parameters listed above, estimates can be made of higher-order (i.e., non-Gaussian) statistical parameters such as skewness, tilt, and kurtosis (peakiness). In practice, however, for a regional study such presented in this paper, only the rms height, orientation of topography, characteristic width and/or plan-view aspect ratio are well-enough resolved that their variation within the study area exceeds the resolution of those parameters. Hence, this study will focus only on those parameters.

NEAR-AXIS DATA

Figures 1 show the track lines of individual swaths in the near-axis data set used for parameter estimation. Segment boundaries were determined by *Tucholke* [1993] on the basis of both bathymetric and backscatter data. These data generally extend from ~1-2 my to ~6-7 Ma crustal ages. The importance of this data set lies in the assumption that

the abyssal hills sampled by these swaths were likely formed by processes similar to those that are now active at zero age. Hence, these data provide us with the best opportunity to correlate abyssal hill characteristics with known ridge characteristics. In this section we present the primary results from this analysis and the comparison of these results with analysis of other geophysical data. Possible implications of these results will be deferred to the Discussion section.

RMS Heights

RMS heights estimated from the near-axis data set (Figure 1) are plotted with 1-σ error bars in Figure 3 as a function of average latitude over the individual swaths. The southern, central and northern segments are identified with different symbols. Two principal observations are noted on this figure. First, the variation in rms heights within each segment is dominated by the inside/outside corner segment offset geometry. The inside corner (west flank) is at the southern end of each segment (Figures 1 and 2). The rms heights are uniformally larger at the inside corners than at the outside corners. However, rms heights do not decrease monotonically going from inside to outside corners. Though not well resolved, the southern segment appears to reach a minimum toward the middle of the segment, similar to observed variations along the EPR flank [*Goff*, 1991; *Goff et al.*, 1993], and the northern segment appears to do just the opposite, finding it's maximum value in the center of the segment.

The second principal observation from Figure 3 concerns the large difference in rms heights between the southern segment and the northern and central segments. Neglecting the inside and outside corners, rms heights within the southern segment are approximately half the rms heights within the central and northern segments. This difference is very striking: the southern segment rms heights are among the lowest values seen in near-axis Atlantic abyssal hill morphology, while rms heights within the adjacent central segment are among the largest (see *Goff* [1991]).

Characteristic Width

Characteristic widths estimated from the near-axis data set (Figure 1) are shown with 1-σ error bars in Figure 4. The characteristic width is not as well-resolved a parameter as rms height, and consequently interpretation of variation in this parameter is less certain. Nevertheless, the following observations may be made. As with rms heights, characteristic widths display an inside/outside corner asymmetry, with the largest characteristic widths tending to occur at the inside corner (southern end of each segment). The central segment displays a nearly monotonic decrease in characteristic width going

from inside to outside corner. In contrast, the southern segment has a well-resolved minimum in the middle of the segment.

Unlike the rms heights, there is little contrast in characteristic width between the southern segment and the central and northern segments. However, the minimum characteristic width for the southern segment is significantly less than the minimum characteristic width for the central and northern segments.

Plan-View Aspect Ratio

Plan-view aspect ratios estimated from the near-axis data set (Figure 1) are shown with 1-σ error bars in Figure 5. Again the variation in this parameter is dominated by the inside/outside corner geometry, with the lowest aspect ratios tending to be at the inside corners. For both the southern and central segments, the aspect ratio near the inner corner approaches unity (i.e., no discernable lineation to the fabric).

Comparison With Other Data

In an effort to obtain clues to the causes for the variations in abyssal hill parameters noted above, here we explore possible correlations with the results of other geophysical and geological analysis. The most consistent variation in all parameters is the inside/outside corner asymmetry (Figures 3, 4, and 5). Inside/outside corner asymmetry is well recognized from other studies of slow-spreading ridges as well [e.g., *Tucholke and Lin*, 1993]. Near axis, inside corners are shallower than outside corners, and faulting at inside corners is more chaotic than at outside corners, where faults are generally parallel to the ridge axis. Off axis, the residual gravity anomaly is larger over inside corner-generated crust than over outside corner-generated crust, implying that inside corner crust is thinner. Dredge samples on outside corner areas frequently contain peridotites and gabbros. These observations support a model in which plate rifting toward the segment ends occurs via a large detachment fault, with the inside corner constituting the footwall and the outside corner the hanging wall. Extrusives erupting at the axis are emplaced principally on outside corner crust, whereas the outside corner consists primarily of deep crustal material associated with the detachment surface [*Tucholke and Lin*, 1993].

The second primary observation is the large contrast in rms heights between the southern segment and the central and northern segments (Figure 3). Inspection of the morphology of the segment axes produces no strong correlations with this observation. Each segment is approximately the same length, has the same inside-outside corner geometry and the offsets north and south of each segment are also similar (see axis traces in Figure 1). Axis depths are shown in the top of Figure 6. Although the central segment

has a peculiarly large deep at its southern end, there is nothing obvious in these profiles to distinguish the southern segment from the northern segment.

Axis mantle Bouger anomalies for these three segments [*Lin ref*], shown in the bottom of Figure 6, do display marked differences between the southern segment and the central and northern segment. Over the southern segment there is a deep low in the mantle Bouger anomaly which in two dimensions is roughly circular in planform (a "bull's eye" gravity low). Mantle Bouger anomalies such as these are interpreted as indicating focused mantle upwelling beneath the axis and/or strong thickening of the crust toward the middle of the segment. It is likely that both are true, since a thicker crust toward the middle of the segment implies greater melt and hence elevated temperatures in the middle relative to the ends of the segment (the argument may be made in either direction). In contrast with the southern segment, the central segment exhibit very weak mantle Bouger low (if at all) toward its center (Figure 6). The large monotonic variation of the mantle Bouger gravity profile across the northern segment is highly anomalous, and an unsolved mystery; perhaps the off-center focus represents an incipient upwelling focus which will, in the near future, rearrange segment boundaries. Nevertheless, it appears that the southern ridge segment, despite similarities in axis length and morphology, is (or was in the recent past) the site of more robust focused upwelling and increased temperatures than the central and northern ridge segments [*Lin ref*].

Evidence that mantle temperatures have been higher at the southern segment is also provided by the off-axis residual gravity anomalies [*Lin Ref*]. These data indicate that for crustal ages up to ~6 my (??), the southern segment has generated crust approximately 1 km thicker than either the central or northern segments. We thus infer that abyssal hill rms heights are correlated with the thermal structure and intensity of mantle upwelling at the ridge axis where they were formed.

Faulting characteristics, as determined with MR1 side-scan data (collected coincident with the Hydrosweep data), also show a marked difference between the southern segment and the central and northern segments (manuscript in preparation by G. Jaroslow). Along a corridor within the middle of each segments and spanning crustal ages ~1-7 Ma, the southern segment exhibits a faulting density of 1.18 ± 0.07 faults/km, whereas the central and northern segments exhibit similar values of 0.76 ± 0.03 faults/km and 0.70 ± 0.02 faults/km respectively. Hence, there appears to a negative correspondence between average rms heights and average faulting densities.

SOUTHERN SEGMENT DATA

Figure 2 shows the track lines of individual swaths in the southern segment data set used for parameter estimation. Of the segments surveyed, only the southern segment has persisted from the western edge of the survey area (~30 Ma crust) to the present day (Figure 2). Hence this segment represents our most complete record of the evolution of a sample spreading ridge through time. There are, however, several complexities to the evolution of the southern segment. At ~11 Ma and ~16 Ma there exist stuctual lineaments which cross-cut the abyssal hill fabric and offset magnetic anomalies (Figure 2). These structures therefore likely represent propagation events, though exactly what caused the propagation is uncertain since both the northern and southern boundaries of the southern segment remained unperturbed at those times [*Kleinrock ref*]. At ~22 Ma plate motions rotated clockwise 8°-10° [*Tucholke*, 1993]. This event coincided with the elimination of a segment to the south of the southern segment. Between ~30 Ma and ~24 Ma the northern boundary of the southern segment is difficult to distinguish. Two possible boundaries are identified [*Tucholke*, 1993] (Figure 2). One or both might have been active, the latter case implying the existence of an additional segment.

Lineament Azimuth

To emphasize the overall behavior of abyssal hill fabric within the southern segment as a function of crustal age, we average the lineament azimuths from the data samples (Figure 2) over 4-5 m.y. age bins. Averaging the results has the added advantage of reducing the size of the errors. Trends estimated in the vicinity of the inside corner are poorly resolved and often highly erratic. To prevent contamination from these values, the two southern-most samples in each age bin were discarded. The resulting averages are plotted in Figure 7. Crustal ages, which are marked at 5 my intervals, range from 0 Ma at the eastern end of the plot to 30 Ma at the western end. Also plotted in Figure 7 is the "normal to flow line" trend estimated from the nearby Kane fracture zone [*Tucholke and Schouten*, 1988]. Neglecting the two age bins likely contaminated by the propagation event (data points plotted at 46°15'W and at 46°50'W; see also Figure 2), the observed abyssal hill lineaments are very consistent with the variation in the Kane fracture zone trend, but shifted clockwise by ~4°-5°.>>>>need mag anom trends<<<<

RMS Height

To emphasize temporal variations over along-axis spatial variations, rms heights estimated from the southern segment data set (Figure 2) are also averaged over 4-5 m.y.

age bins. To maintain consistency with lineament azimuths, the southernmost two data points in each age bin were discarded. Averaged rms heights are plotted with 1-σ error bars as a function of longitude in Figure 8a. The horizontal bars represent the approximate range in longitude sampled by each averaging bin. The principal observation to be noted from this plot is the significant variation in rms hight on time scales ranging from ~5-15 my. The large rms height values in the 7-12 Ma range are undoubtably due in part by the possible pseudofault running through this region. However, the subsequent 12-17 Ma range also contains a possible pseudofault, yet exhibits some of the lowest rms heights. Hence, while the orientation of abyssal hills may be significantly affected by these cross-cutting structures, the size of abyssal hills appear predominantly affected by other factors.

Individual rms heights are plotted as a function of swath latitude in Figure 9 for age ranges 17-21 Ma, 21-25 Ma, and 25-29 Ma. The samples in the 25-29 Ma age range cross one of the tentative boundaries identified by *Tucholke* [1993]. Along-axis variation in rms height displays a similar character within each of these three age ranges. As with the near-axis data (Figure 3), there is a clear asymmetry associated with the inside/outside corner geometry of the segment, with larger rms heights at the inside corner (southern end of segment). However, the pattern of rms heights plotted in Figure 9 display an added feature not seen on the near axis plots (Figure 3): proceding from inside to outside corner (north to south), the rms heights at first decrease, then increase marginally toward the middle before decreasing again toward the outside corner. Though the error bars are generally large relative to this small increase in rms height, the consistancy of this feature at all three age ranges suggests that it is real. The rms height increase in the 25-29 Ma range is spatially coincident with *Tucholke's* [1993] tentative identification of a possible segment boundary.

Characteristic Width and Plan-View Aspect Ratio

Characteristic widths estimated from the southern segment data set (Figure 2), and averaged in the same manner as lineament azimuths and rms heights, are plotted in Figure 10a. The variation in this parameter is similar to the rms height estimates (Figure 8a). The clearest positive correlation between rms height and characteristic width is seen in the large increase in both parameters going from the 1-7 Ma range to the 7-12 Ma range, and then the large decrease in both parameters to the 12-17 Ma range. There is also a well-resolved increase in rms height and charcteristic width going from the 21-25 Ma range to the 25-29 Ma range. However, the change going from the 17-21 Ma range to the

21-25 Ma range is marginally negative for characteristic width while well-resolved positive for rms height.

Individual estimations of characteristic width in the age range 17-29 Ma are, like the rms heights, generally larger at the inside corners than the outside corners. However, no obvious increase in this parameter is observed toward the middle of the segment as there appears to be in the rms heights (Figure 9). The degree of positive correlation between rms height and characteristic width is most objectively quantified by the correlation coefficient. For either the entire data set or just the southern segment data set the correlation coefficient between these two parameters is +0.48 with confidence >99%. Though this coefficient is not very high, it is well resolved and represents a minimum value since the actual correlation is degraded by random errors in both parameters. Hence, it is likely that both characteristic width and rms height are being influenced in a similar manner.

Figure 10*b* plots plan-view aspect ratios estimated from the southern segment data set (Figure 2), and averaged in the same manner as with all previous parameters. The pattern expressed in this plot is similar and opposite to the plots of averaged rms height, residual gravity and characteristic width in Figures 8 and 10*a*.

As with the near-axis samples, individual estimations of plan-view aspect ratios over the entire southern segment are almost uniformally smallest near the outside corner. To quantify this observation we have calucated the average aspect ratio for the southern two swaths for every segment and every age range shown on Figures 1 and 2 and also calculated the average over all remaining swaths. The near-inside corner swaths have an average aspect ratio of 2.04 ± 0.18, and the remaining samples have an average aspect ratio of 3.70 ± 0.21, almost a factor of 2 difference.

Comparison With Other Data Sets

As with our analysis of near-axis abyssal hill morphology, we find a primary correlation between gravity and rms heights within the southern segment. Figure 8*b* shows residual gravity within the southern segment; each plotted value represents the average residual gravity over the identical regions used in the estimation of rms height in Figure 8*a* (data from *Lin ref*). The positive correlation between these two plots is clear and robust. The only slight difference between thee two is that the rms heights in the 7-12 Ma range are slightly large relative to the corresponding residual gravity anomaly (perhaps an additional effect the pseudofault running through this region (Figure 2)). As stated before, residual gravity anomalies are interpreted as reflecting the thickness of the crust: residual lows imply thicker crust and highs imply thinner crust. Variations in

thickness of the crust are, in turn, indicative of variations in mantle temperature at the axis at the time of emplacement [*Lin ref*]. Hence, we infer that the rms height of abyssal hills are influenced by temporal variations in mantle upwelling at the ridge axis: where the temperature is relatively hot and thicker crust produced, abyssal hill rms height is relatively low, and where the temperature is relatively cold and thinner crust produced, abyssal hill rms height is relatively high.

The correlation between residual gravity and abyssal hill characteristics may also be demonstrated on unaveraged estimates. For example, over the entire data set, the correlation coefficient between residual gravity and rms height is $\rho = +0.57$ with confidence >99%. In addition to reflecting flow-line variations in gravity and rms height, this correlation is also consistent with inside/outside corner asymmetry (larger rms heights and thinner crust at inside corners). Though less robust, correlations can also be demonstrated between residual gravity and both characteristicwidth ($\rho = +0.31$, confidence = 99%) and plan-view aspect ratio ($\rho = -0.33$, confidence = 99%).

The negative corresopondence noted earlier between near-axis abyssal hill rms and faulting structure (as revealed in the MR1 side-scan data) cannot be demonstrated for the southern segment data set. Figure 11*a* plots average faulting densities with standard errors calculated along a corridor within the center of the southern segment. The same age ranges as with the abyssal hill analysis were used. While the large decrease in faulting density from the 2-7 Ma range to the 7-12 Ma range is consistent with the large increase in rms height over the same age range (Figure 8*a*), variation in faulting densities at older crustal ages clearly do not negatively correspond with rms height. This lack of correspondence may be related to sedimentation. Figure 11*b* plots average sediment loads over the southern segment as derived from estimates presented by *Webb and Jordan* [1993]. *Webb and Jordan* [1993] created a highly innovative approach to sediment chatacterization based on realistic numerical sedimentation algorithms. They find that sediment load does not increase monotonically with age, but rather reaches a peak at ~50 m in the range 15-20 Ma before decreasing to ~25 m at ~25 Ma. This observation is qualitatively consistent with single channel data collected in the same region, and may be explained by an hypothesized change in the carbonate compensation depth in the late Miocene [*Webb and Jordan*, 1993]. Sediment loads will, of course, cover the smaller faults from side-scan detection, hence decreasing the apparent faulting density. This fact may help explain the negative correspondence between faulting densities (Figure 11*a*) and *Webb and Jordan*'s [1993] estimates of sediment load (Figure 11*b*) at crustal ages beyond 12 Ma.

We also note that the ~25 m decrease in sediment load from ~17 Ma to ~25 Ma (Figure 11*b*) may partially explain the variation in rms height over the same age range (Figure 8*a*). However, Webb (personal communication, 1993) estimates that, even for the highly ponded sediments within the study area, an average sediment load of *L* will decrease the topographic rms height by only ~*L*/2. Hence, sedimentation is likely not a significant factor in the ~120 increase in average rms height from ~17 Ma to ~29 Ma.

CONCLUSIONS AND DISCUSSION

The results of the statistical analysis of the ARSRP Hydrosweep data can be simplified to the following primary observations: (1) Abyssal hill morphology in the both the near-axis and 17-29 Ma southern segment data sets is strongly influenced by the inside/outside corner geometry of the mid-ocean ridge segments; inside corners produce abyssal hills with larger rms height and characteristic width and smaller plan-view aspect ratios than abyssal hills produced at outside corners. (2) Though there is an overall decrease in rms height going from inside to outside corner in the 17-29 Ma range of the southern segment, there is a slight increase in this parameter toward the middle of the segment. In the 25-29 Ma range this increase correlates with the tentative segment boundary identified by *Tucholke* [1993]. (3) Along the southern segment flow line, lineament azimuths, where not affected by evident propagator structures or inside corners, are generally perpendicular to the anticipated flow line???????>>>>need mag anom trends<<<<(4) Both the inter-segment and flow-line variation in rms height and, to a much lesser extent, characteristic width of abyssal hills are positively correlated with residual gravity anomaly. This implies that smaller abyssal hills are produced when the crust being generated is thicker (i.e., when the mantle beneath the axis is hotter) and larger abyssal are produced when the crust being generated is thinner (i.e., when the mantle beneath the axis is colder). (5) Variations in average near-axis rms heights over the three segments negatively correspond with variations in average faulting density as determined from analysis of MR1 side-scan imagery. This is circumstantial evidence supporting the assertion that faulting plays a dominant role in abyssal hill formation at slow spreading rates. However, a negative correspondence between rms height and faulting density is not generally observed in the flow-line data of the southern segment. This may be attributable to sedimentation effect.

Below we present discussion and conjecture related to these observations.

Abyssal Hill Segmentation

Goff [1991] has documented numerous textural differences between MAR- and EPR-produced abyssal hills. To these differences we add another: the response of abyssal hills to mid-ocean ridge segmentation. Along the flanks of the EPR, abyssal hills appear to vary in response to the upwelling structure beneath the ridge segment, with smaller rms height toward the middle of segments and larger rms height toward the ends [*Goff*, 1991; *Goff et al.*, 1993]. In contrast, within the MAR segments surveyed, along-axis variation in abyssal hill rms height predominantly correlates with the inside/outside corner offset geometry.

This difference in the response of MAR- and EPR-produced abyssal hills to ridge segmentation is very similar in some respects to the differences in MAR- and EPR ridge segments. Both MAR and EPR segments respond to temperature variations associated with focussed upwelling: the MAR axis tends to be shallowest toward the middle of segment and deepest toward the ends [e.g., *Macdonald et al.*, 1991], and the EPR axial high tends to be wider and shallower toward the segment middle and thinner and shallower toward segment ends [*Macdonald and Fox*, 1988; *Cochran et al*, 1993]. However, of the two only MAR segments display a significant inside/outside corner asymmetry. MAR inside corner crust is thinner than outside corner crust, often perhaps with no extrusive basalt layer [*Tucholke and Lin*, 1993]. Deep tow studies suggest that the basement surface generated at inside corners is a low-angle detachment fault which is later broken up by secondary high-angle normal faulting [*Tucholke and Lin*, 1993; and references therein]. These observations suggest a model where the rift valley near the end of a segment is maintained as a half graben, with most of the volcanic output being deposited on the hanging wall (the outside corner) and then additionally faulted rafted away [*Tucholke and Lin*, 1993]. The footwall brings deeper crustal, and occaisionally mantle material to the surface where it too is additionally faulted and rafted away [*Tucholke and Lin*, 1993]. Two factors are evident in these models which will affect inside/outside corner surface morphology: (1) crustal thickness and composition vary significantly between inside and outside corner, which will have an effect on the response of normal faulting to extenstion, and (2) volcanic edifice formation will significantly differ between inside and outside corners. The inside/outside corner asymmetry in abyssal hill characteristics (Figures 3, 4, and 5) suggests that one or both of these factors significantly influences the formation of abyssal hills.

The slight increase in rms height noted in the middle of the southern segment in the 17-29 Ma range (Figure 9) supports the tentative segment boundary identification of *Tucholke* [1993] (Figure 2); i.e., what we are including in the "southern segment" category at the oldest crustal ages sampled might actually consist of two segments

separated by a small-offset discontinuity. However, it also suggests that, rather than dying out ~25 Ma or merging with the possible segment boundary located just to the north (Figure 2), this segment boundary persisted as a small or zero-offset segment boundary up to ~17 Ma. As one possible scenario, we suggest that such a segment boundary might help explain the existence of one or both of the apparent propagator psuedofaults which are observed at ~11 Ma and 16 Ma.

Abyssal Hills and Mantle Upwelling

While intra-segment variation is dominated by an inside/outside corner asymmetry, inter-segment and flowline rms height variation is strongly coupled to the spatial and temporal variations in axis temperature structure that existed at the time of abyssal hill formation as inferred from residual gravity anomalies. EPR-produced abyssal hills are also coupled to axis thermal structure, but this correlation is observed primarily at the intra-segment scale. RMS heights on EPR flanks tend to be smallest toward the middle of the segment and increase toward the ends; a pattern which correlates with the focusing of mantle upwelling beneath the ridge axis [*Goff*, 1991; *Goff et al.*, 1993]. MAR abyssal hills may also be influenced by the focusing of mantle upwelling beneath the ridge segment, but if so this signal is obscured by the inside/outside corner asymmetry. The small minimum in rms height in the near axis swaths of the southern segment (Figure 4) may be one possible example of the superposition of abyssal hill response to inside/outside corner asymmetry and focused mantle upwelling. We anticipate that as the axis temperature increases, the abyssal hill response to focused mantle upwelling will increase at the expense of inside/outside corner asymmetry.

The connection between abyssal hill rms heights and axis temperature is intuitively reasonable, though the details and dynamic modeling are likely to be quite difficult. Differences in ridge temperature imply differences in the elastic thickness of the lithosphere [*McNutt*, 1984]. This will have at least two possible effects on normal faulting associated with lithospheric extension: (1) near-axis faults can extend deeper cooler ridges and a greater fault throw can accommodate crustal extension before another fault must be created [*Forsyth*, 1992] and (2) the greater strength associated with a cooler ridge will increase the size of the axial rift valley [*Tapponnier and Francheteau*, 1978; *Phipps-Morgan et al.*, 1987; *Lin and Parmentier*, 1989; *Chen and Morgan*, 1990], which must be accomodated by surface normal faulting. Differences in termperature may also have an influence on the style of surface volcanism. *CYAMEX* [1981] noted that at slow spreading ridges volcanic edifices are commonly generated, whereas at fast spreading ridges sheet flows are more common. Assuming that differences in styles of mid-ocean

ridge volcanism are predominantly temperature related, this suggests that volcanism would tend to contribute more to the rms height of abyssal hills where the axis temperature structure is colder.

Abyssal Hills and Faulting

The correlation between rms height and faulting density in the near-axis (low sediment) data sets provides strong circumstantial evidence that abyssal hills within this survey area are predominantly fault-generated. Whether MAR abyssal hills are generated predominantly by faulting processes or volcanic processes has been debated rather vigorously in the literature. *Rona et al.* [1974] concluded from a study of abyssal hills east of the MAR near 23°N that both volcanic and tectonic processes play an important role in their formation. *Kong et al.* [1988] and *Pockalny et al.* [1988] observed that a large volcanic edifice formed in the rift valley near 23°N was similar in size and shape to abyssal hill structures off-axis, and thus proposed that abyssal hills in this region are extinct volcanic edifices which have been rafted away. However, before a volcanic edifice can be rafted away, it must pass over the rift mountains, and in the process be subjected to severe normal faulting with individual fault throws on the order of hundreds of meters [*Macdonald and Luyendyk*, 1977]. *Smith and Cann* [1990] suggest that such faulting so drastically alters surface morphology that volcanic edifices constructed within the median valley can no longer be identified as distinct features following the faulting process. While we prefer to think that many volcanic features may exit the rift valley intact, the evidence does lead us to suggest that normal faults are the dominant abyssal-hill forming structures, and that any successfull model of abyssal hill formation must take faulting into account.

REFERENCES

Bell, T. H., Statistical features of sea-floor topography, *Deep Sea Res.*, 22, 883–892, 1975*b*.

Bell, T. H., Mesoscale sea floor roughness, *Deep Sea Res.*, 26A, 65–76, 1978.

Bicknell, J. D. J.-C. Sempere, K. C. Macdonald, and P. J. Fox, Tectonics of a fast spreading center: A Deep-Tow and Sea Beam survey on the East Pacific Rise at 19° 30' S., *Mar. Geophys. Res.*, 9, 25-45, 1987.

Chayes, D. N., D. W. Caress, W. B. F. Ryan, A. Malinverno, W. Menke, and C. Keely, Status of Hydrosweep on the R/V Ewing: System operation and data processing, *Eos Trans. AGU*, 72, 488, 1991.

Chen, Y., and W. J. Morgan, Rift valley/no rift valley at mid-ocean ridges, *J. Geophy. Res.*, *95*, 17,571-17,581, 1990.

Cochran, J. R., J. A. Goff, A. Malinverno, D. J. Fornari, C. Keeley, and X. Wang, Morphology of a "superfast" mid-ocean ridge crest and flanks: The East Pacific Rise, 7°-9°S, *Mar. Geophys. Res.*, in press, 1992.

CYAMEX, First manned submersible dives on the East Pacific Rise at 21°N (project RITA): General results, *Mar. Geophys. Res.*, *4*, 345-379, 1981.

Forsyth, D. W., Finite extension and low-angle normal faulting, *Geology*, *20*, 27-30, 1992.

Fox, C. G., and D. E. Hayes, Quantitative methods for analyzing the roughness of the seafloor, *Rev. Geophys.*, *23*, 1–48, 1985.

Gilbert, L. E., and A. Malinverno, A characterization of the spectral density of residual ocean floor topography, *Geophys. Res. Lett.*, *15.*, 1401-1404, 1988.

Goff, J. A., and T. H. Jordan, Stochastic Modeling of Seafloor Morphology: Inversion of Sea Beam data for second-order statistics, *J. Geophys. Res.*, *93*, 13 589-13 608, 1988.

Goff, J. A., and T. H. Jordan, Stochastic Modeling of Seafloor Morphology: resolution of topographic parameters by Sea Beam data, *IEEE J. Ocean Eng.*, *14*, 326-337, 1989.

Goff, J. A., Stochastic Modeling of Seafloor Morphology (Ph.D. Thesis), Massachusetts Institute of Technology/Woods Hole Oceanographic Institution, Cambridge, 266 pp., 1990.

Goff, J. A., A global and regional stochastic analysis of near-ridge abyssal hill morphology,*J. Geophys. Res.*, *96*, 21,713-21,737, 1991.

Goff, J. A., Quantitative characterization of abyssal hill morphology along flow lines in the Atlantic Ocean, *J. Geophys. Res.*, *97*, 9183-9202, 1992.

Goff, J. A., A. Malinverno, D. J. Fornari, and J. R. Cochran, Abyssal hill segmentation: quantitative analysis of the East Pacific Rise flanks 7°S-9°S, *J. Geophys. Res.*, in press, 1993.

Hayes, D. E., and K. A. Kane, The dependence of seafloor roughness on spreading rate, *Geophys. Res. Let.*, *18*, 1425-1428, 1991.

Kong, L. S. L., R. S. Detrick, P. J. Fox, L. A. Mayer, and W. B. F. Ryan, The morphology and tectonics of the MARK area from Sea Beam and Sea MARC I observations (Mid-Atlantic Ridge 23° N), *Mar. Geophys. Res.*, *10*, 59-90, 1988.

Krause, D. C., and H. W. Menard, Depth distribution and bathymetric classification of some seafloor profiles, *Mar. Geol.*, *3*, 169–193, 1965.

Lin, J., and E. M. Parmentier, Mechanims of lithospheric extension at mid-ocean ridges, *Geophys. J.*, *96*, 1-22, 1989.

Lonsdale, P., Structural geomorphology of a fast-spreading rise crest: The East Pacific Rise near 325'S, *Mar. Geophys. Res., 3,* 251-293, 1977.

Macdonald, K. C., Mid-ocean ridges: fine scale tectonic, volcanic and hydrothermal processes within the plate boundary zone, *Ann. Rev. Earth Planet. Sci., 10,* 155-190, 1982.

Macdonald, K. C., and B. P. Luyendyk, Deep-tow studies of the structure of the Mid-Atlantic ridge near lat 37° N., *Geol. Soc. Am. Bull., 88,* 621–636, 1977.

Macdonald, K. C., and P. J. Fox, The axial summit graben and cross-sectional shape of the East Pacific Rise as indicators of axial magma chambers and recent volcanic eruptions, *Earth Planet. Sci. Lett., 88,* 119-131, 1988.

Macdonald, K. C., D. S. Scheirer, and S. M. Carbotte, Mid-Ocean Ridges: Discontinuities, segments and giant cracks, *Science, 253,* 986-994, 1991.

Malinverno, A., Inverse square-root dependence of mid-ocean-ridge flank roughness on spreading rate, *Nature, 352,* 58-60, 1991.

Malinverno, A., and R. A. Pockalny, Abyssal hill topography as an indicator of episodicity in crustal accretion, *Earth Planet. Sci. Lett., 99,* 154-169, 1990.

Malinverno and Cowie, 1993.

McDonald, M. F., and E. J. Katz, Quantitative method for describing the regional topography of the ocean floor, *J. Geophys. Res., 74,* 2597–2607, 1969.

McNutt, M. K., Lithospheric flexure and thermal anomalies, *J. Geophys. Res., 89,* 11,180-11,194, 1984.

Menard, H. W., Sea floor spreading, topography and the second layer, *Science, 157,* 923-924, 1967.

Menard, H. W., and J. Mammerickx, Abyssal hills, magnetic anomalies and the East Pacific Rise, *Earth Plan. Sci. Lett., 2,* 465-472, 1967.

Phipps-Morgan, J., E. M. Parmentier, and J. Lin., Mechanisms for the origin of mid-oceanic ridge axial topography: Implications for the thermal and mechanical structure of accreting plate boundaries, *J. Geophys. Res., 92,* 12,823-12,836, 1987.

Pockalny, R. A., R. S. Detrick, and P. J. Fox, Morphology and tectonics of the Kane transform from Sea Beam bathymetry data. *J. Geophys. Res., 93,* 3179-3193, 1988.

Rognstad, M, HAWAII MAR: A new underwatter mapping tool, *International Conference on Signal Processing Applications and Technology,* Fall, 1992.

Rona, P. A., R. N. Harbison, and S. A. Bush, Abyssal hills of the eastern central north Atlantic, *Mar. Geol., 16,* 275-292, 1974.

Schouten, H., and C. Denham, Deconvolution of faulted normal seafloor in the North Atlantic FAMOUS area (abstract), *Eos Trans. AGU, 64,* 314, 1983.

Smith, D. K., and J. Cann, Hundreds of small volcanoes on the median valley floor of the Mid-Atlantic Ridge at 24°-30°N, *Nature, 348,* 152-155, 1990.

Tapponnier, P., and J. Francheteau, Necking of the lithosphere and mechanics of slowly accreting plate boundaries, *J. Geophys. Res., 83,* 3955-3970, 1978.

Tucholke, B. E., and H. Schouten, Kane Fracture Zone, *Mar. Geophys. Res., 10,* 1-39, 1988.

Tucholke, B. E., K. C. Macdonald, and P. J. Fox, ONR seafloor natural laboratories on slow- and fast-spreading mid-ocean ridges, *Eos Trans. AGU, 72,* 268-270, 1991.

Tucholke, not yet submitted to Nature, 1993.

Tucholke, B. E., and J. Lin, A geologic model for the structure of ridge segments in slow-spreading ocean crust, submitted to *J. Geophys. Res.,* 1993.

Webb, H. F., and T. H. Jordan, Quantifying the distribution and transport of pelagic sediments on young abyssal hills, *Geophys. Res. Lett., 20,* 2203-2206, 1993.

FIGURES

Fig. 1. Locations of the near axis swath data sets described in the text (line segments terminated by dots) and map of the primary structural features surveyed by the EW9208 ARSRP geophysical reconnaissance cruise (see *Tucholke* [1993]). The swath data sets are sampled from the gridded data and are 7.5 km in width. Dashed lines indicate tentatively identified structures.

Fig. 2. Locations of the south segment data sets described in the text (line segments terminated by dots) and map of the primary structural features surveyed by the EW9208 ARSRP geophysical reconnaissance cruise (see *Tucholke* [1993]). The swath data sets are sampled from the gridded data and are 7.5 km in width. Dashed lines indicate tentatively identified structures. Approximate crustal ages at the swath data termination points are also given.

Fig. 3. RMS heights estimated from the near axis swath data samples (Figure 1) plotted as a function of average latitude over the length of the swath. Vertical bars represent 1-σ error estimates.

Fig. 4. RMS heights estimated from the near axis swath data samples (Figure 1) plotted as a function of average latitude over the length of the swath. Vertical bars represent 1-σ error estimates.

Fig. 5. Plan-view aspect ratios estimated from the near axis swath data samples (Figure 1) plotted as a function of average latitude over the length of the swath. Vertical bars represent 1-σ error estimates.

Fig. 6. (*a*) Axis topography along the Mid-Atlantic Ridge through the survey area. (*b*) Mantle Bouger anomaly sampled at the axis of the three segments of the study area [*Lin ref*].

Fig. 7. Lineament azimuths averaged within each age range over the south segment swath data samples (Figure 2) plotted as a function of average longitude. Vertical bars represent 1-σ error estimates on the averages. Horizontal bars represent the approximate longitudinal span of the samples. Crustal ages are also indicated.

Fig. 8. (*a*) RMS heights averaged within each age range over the south segment swath data samples (Figure 2) plotted as a function of average longitude. Vertical bars represent 1-σ error estimates on the averages. Horizontal bars represent the approximate longitudinal span of the samples. Crustal ages are also indicated. (*b*) Residual gravity within the southern segment; each plotted value represents the average residual gravity over the identical regions used in the estimation of rms height in (*a*) (data from *Lin ref*).

Fig. 9. Individual rms heights for age ranges (*a*) 17-21 Ma, (*b*) 21-25 Ma, and (*c*) 25-29 Ma, south segment plotted as a function of swath latitude. A possible location of a segment boundary (see text) is also marked on each.

Fig. 10. (*a*) Characterstic widths and (*b*) plan-view aspect ratios averaged within each age range over the south segment swath data samples (Figure 2) plotted as a function of average longitude. Vertical bars represent 1-σ error estimates on the averages. Horizontal bars represent the approximate longitudinal span of the samples. Crustal ages are also indicated.

Fig. 11. (*a*) Average fault densities within each south segment age range (Figure 2) plotted as a function of average longitude. Fault densities were calculated from MR1 side-scan data along a flow-line corridor approximately within the center of the south segment. Vertical bars represent 1-σ error estimates on the averages. Horizontal bars represent the approximate longitudinal span of the samples. Crustal ages are also

indicated.   (*b*) Average sediment loads over the south segment (from *Webb and Jordan* [1993]).
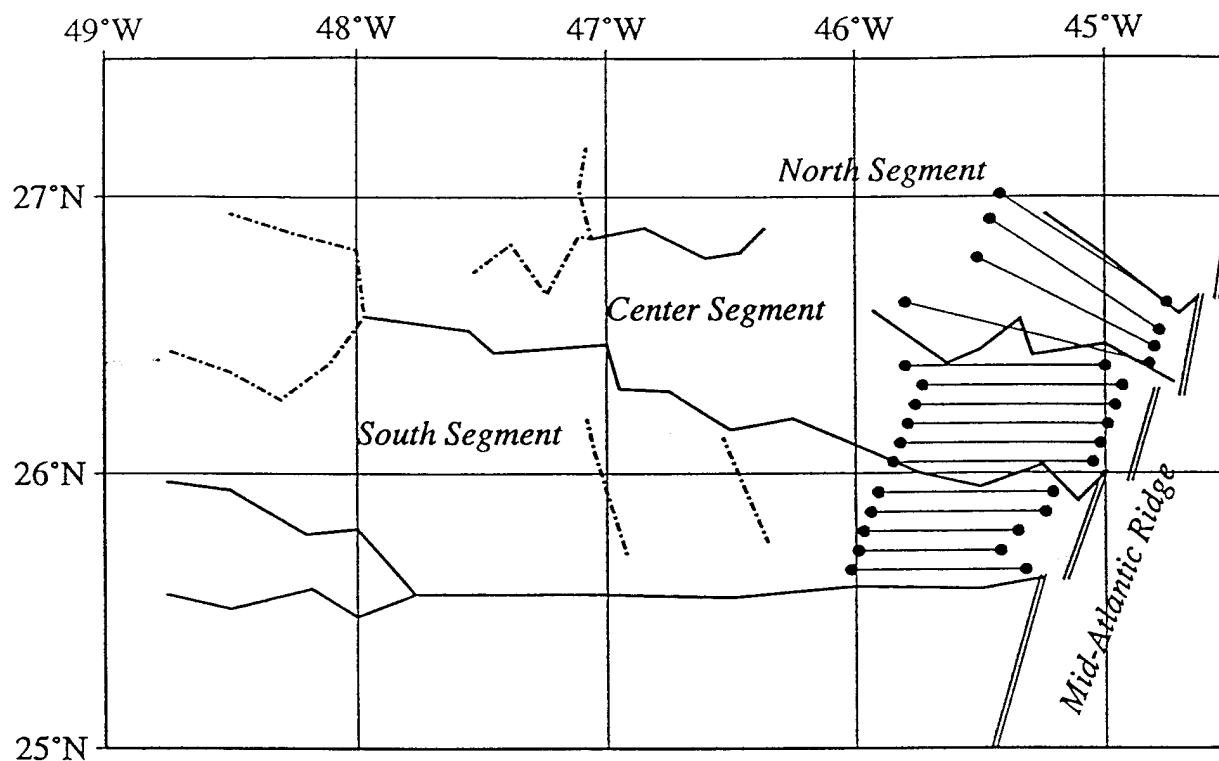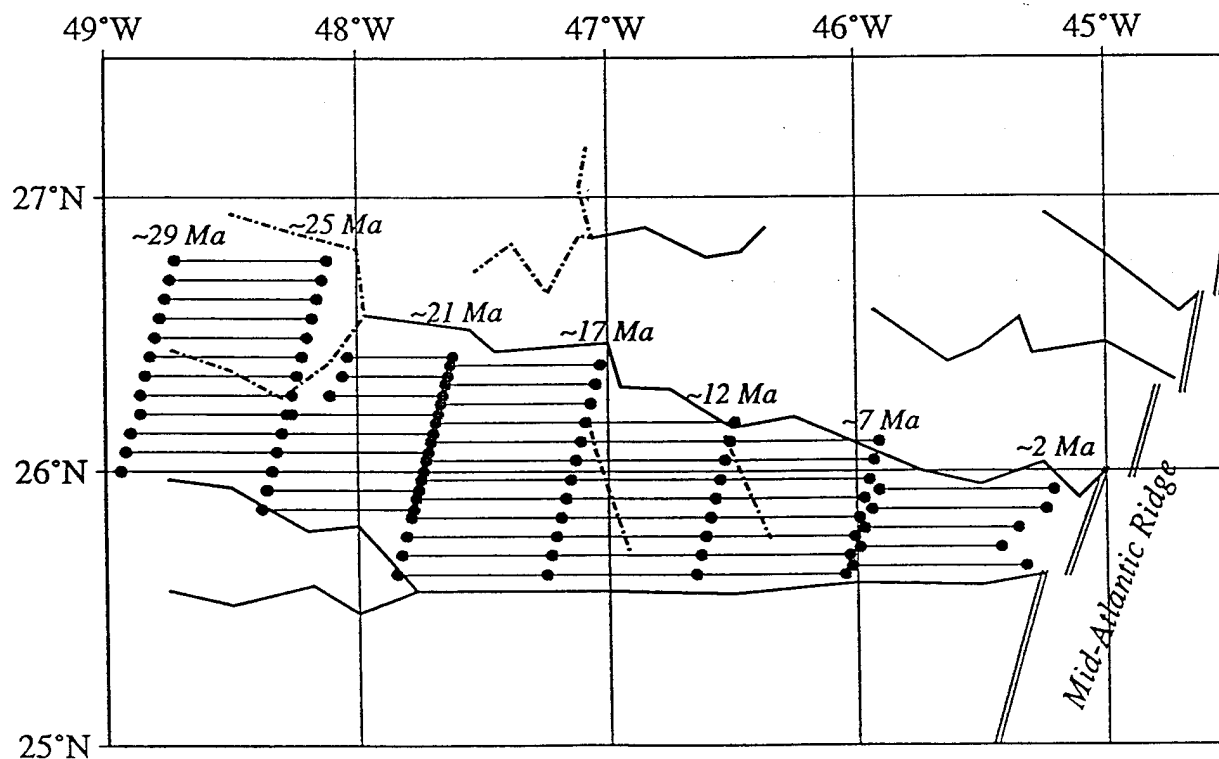
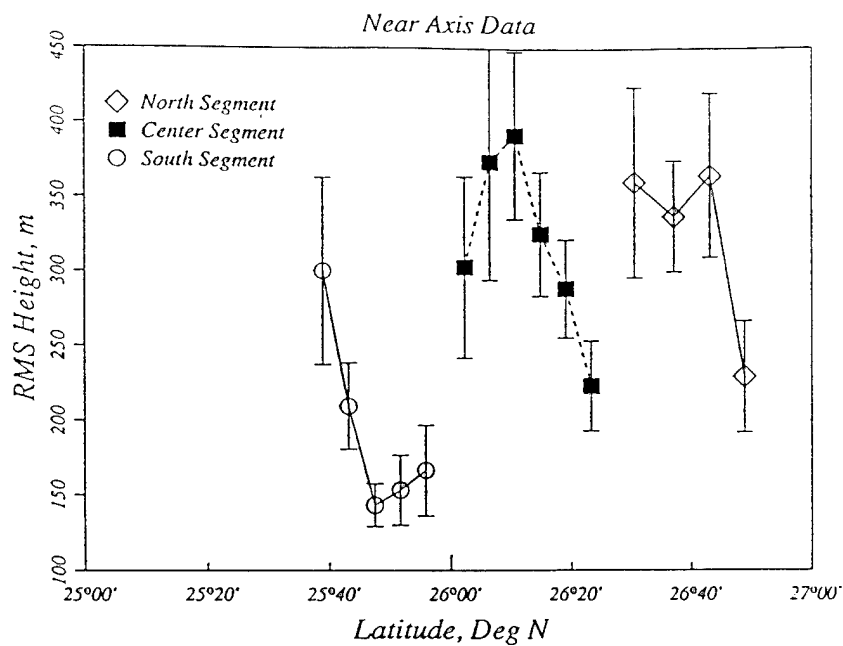# Near Axis Data

Figure 1

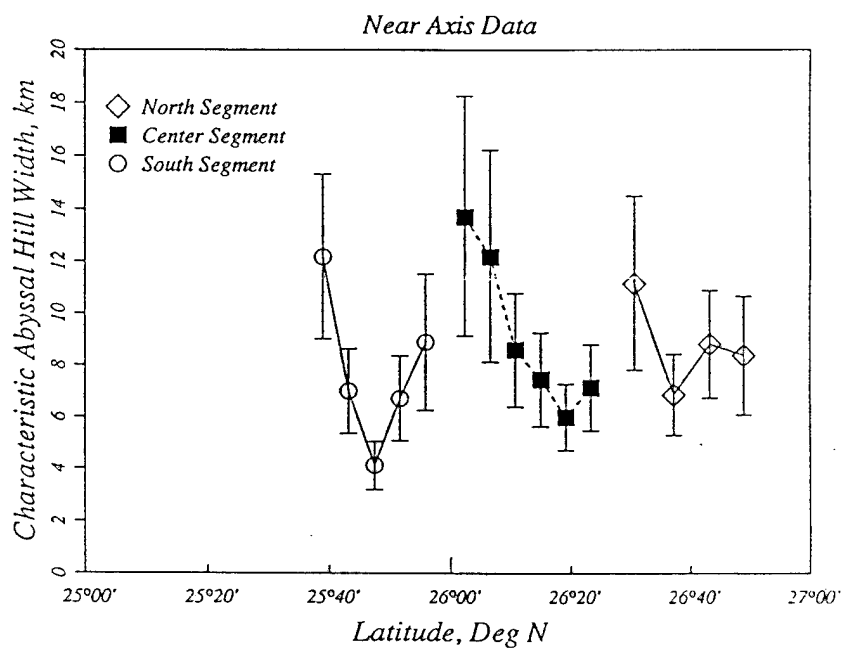# South Segment Data

Figure 2

Figure 3

Figure 4

Figure 5

Axis Depth

a.

b.
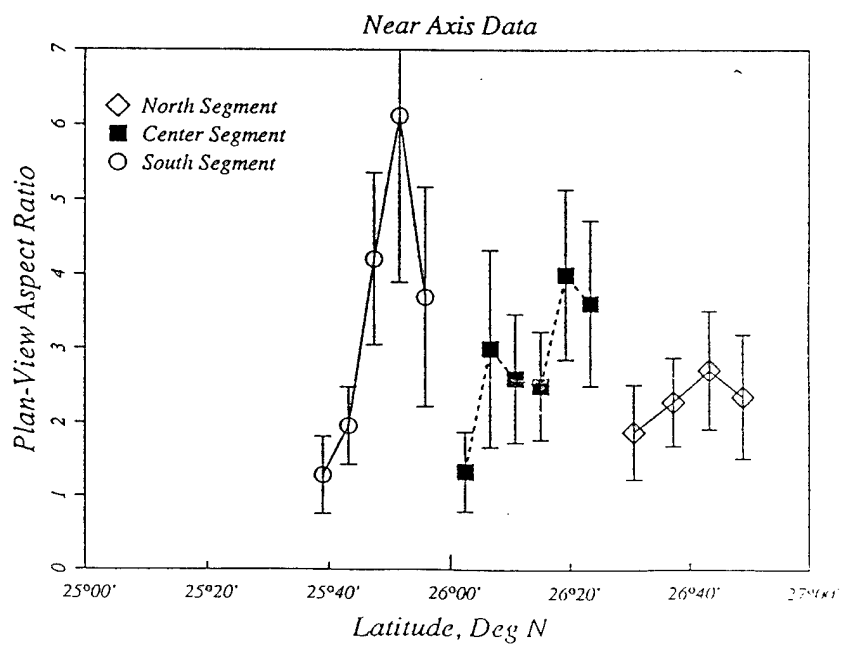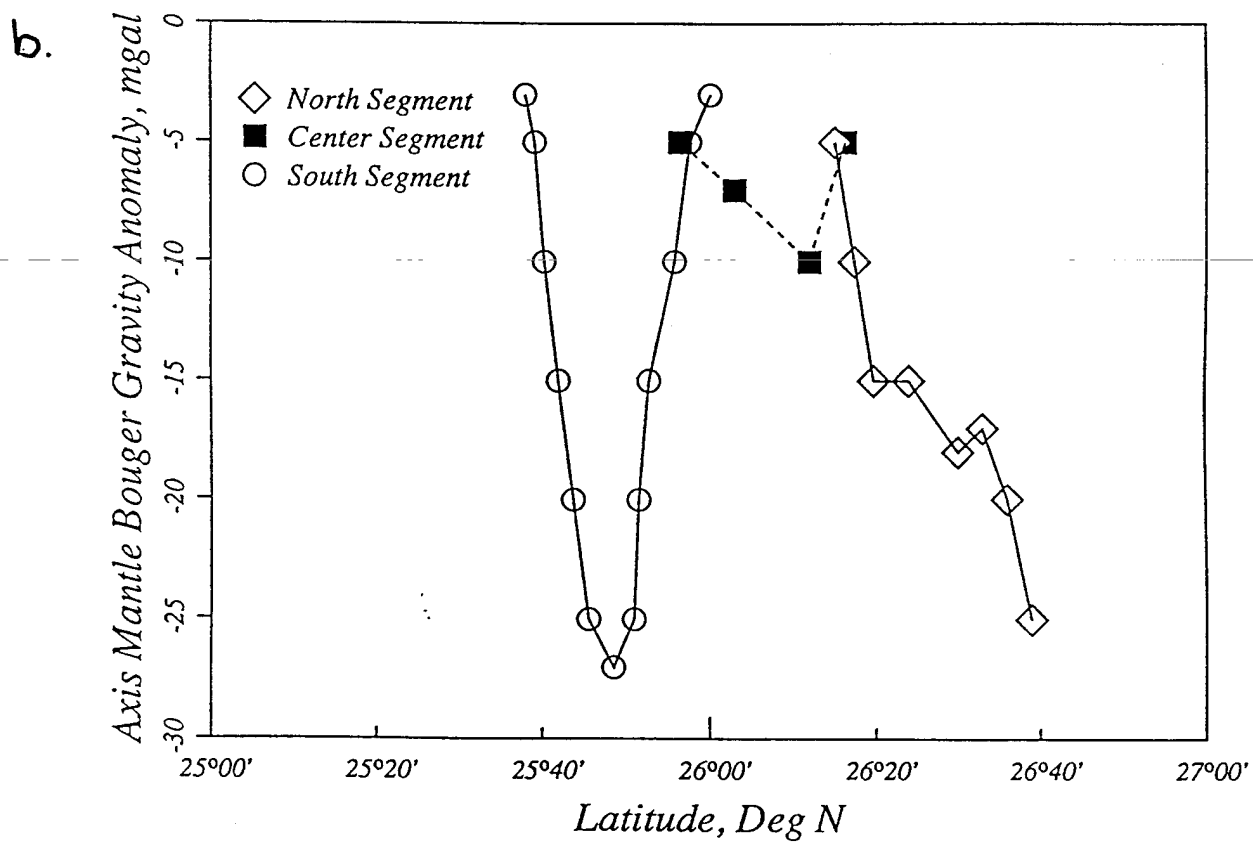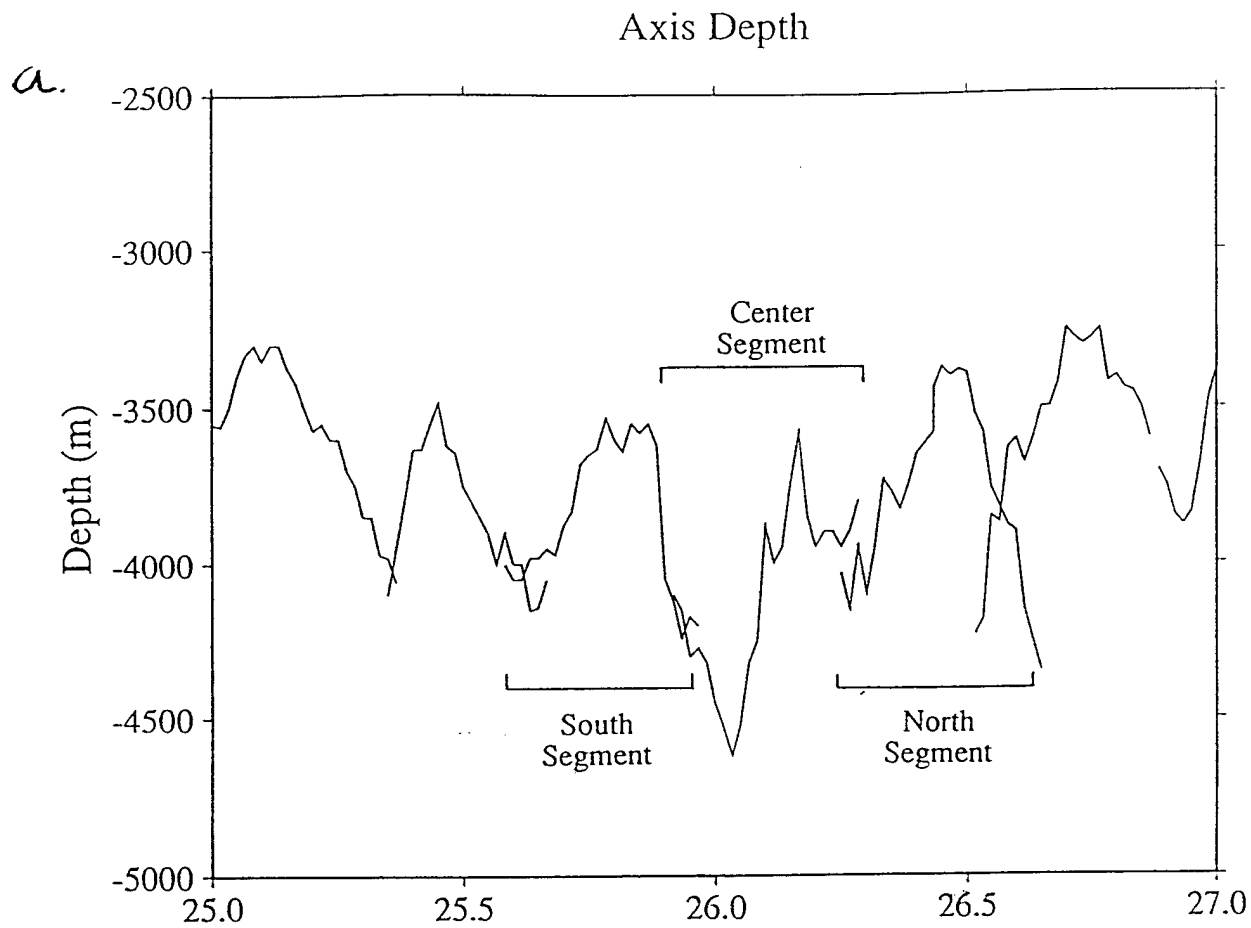
Figure 6
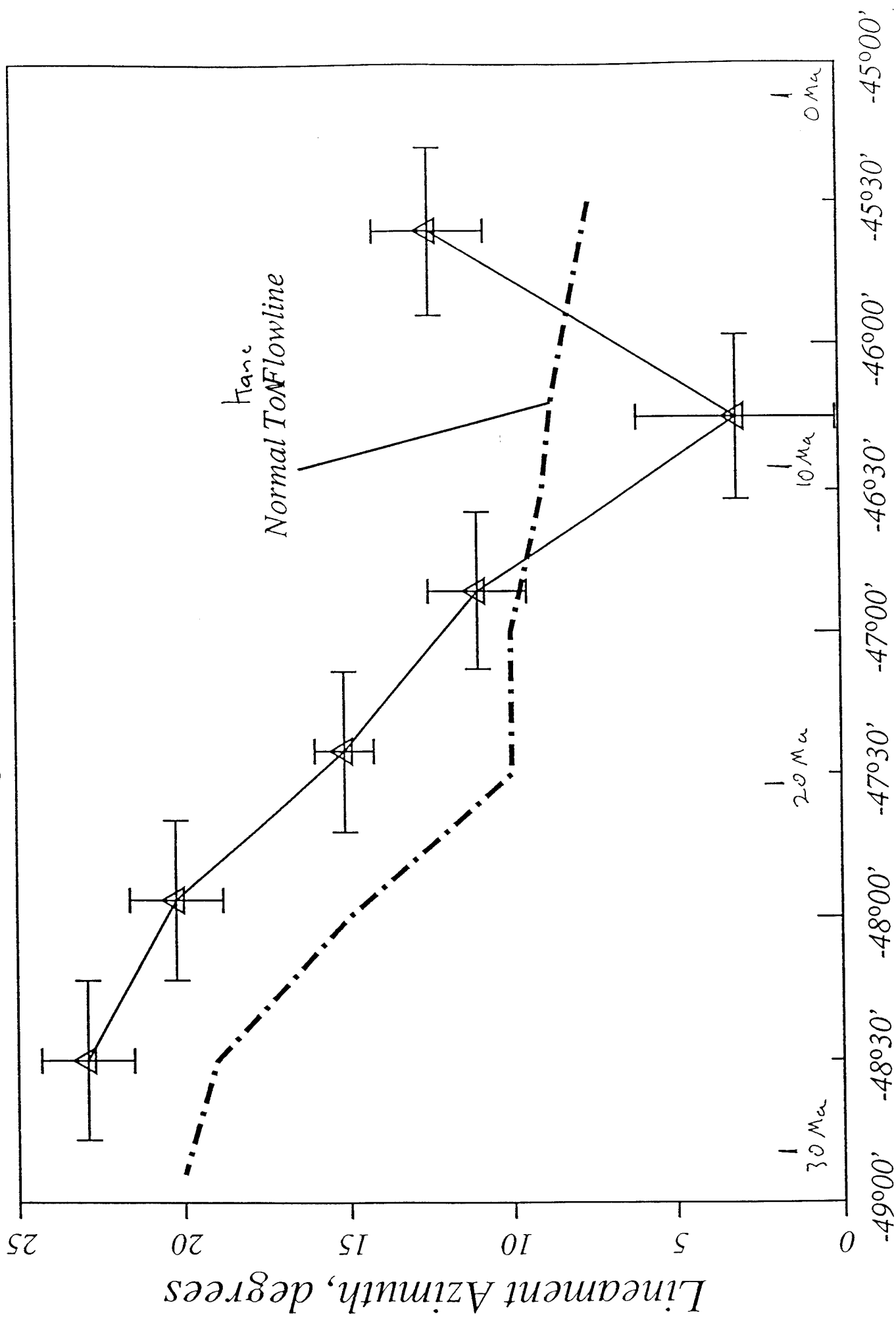
South Segment, 4-5 M.Y. Averages

Figure 7

South Segment 4-5 m.y. Averages

a.

b.

Figure 8
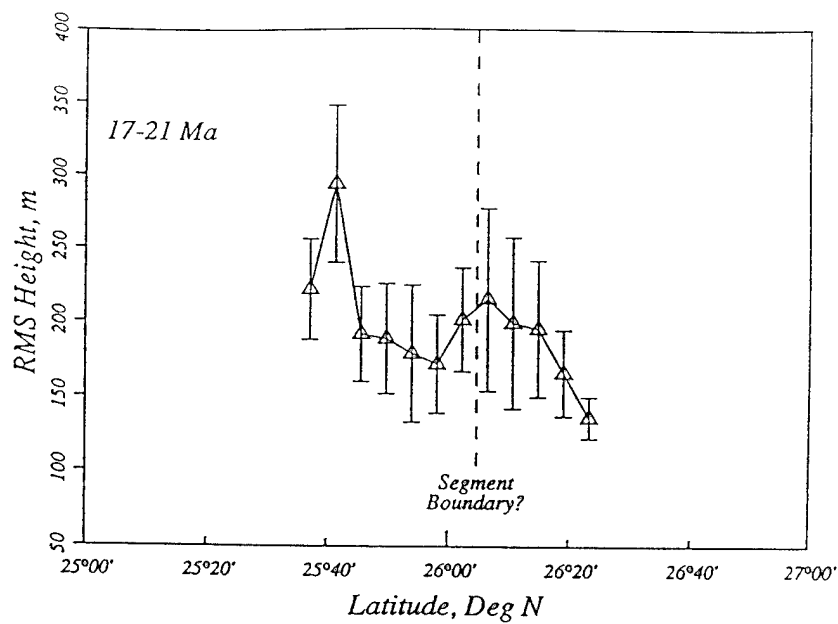
a.

17-21 Ma

RMS Height, m vs *Latitude, Deg N*

Segment Boundary?

b.

21-25 Ma

RMS Height, m vs *Latitude, Deg N*

Segment Boundary?

c.

25-29 Ma

RMS Height, m vs *Latitude, Deg N*

Segment Boundary?
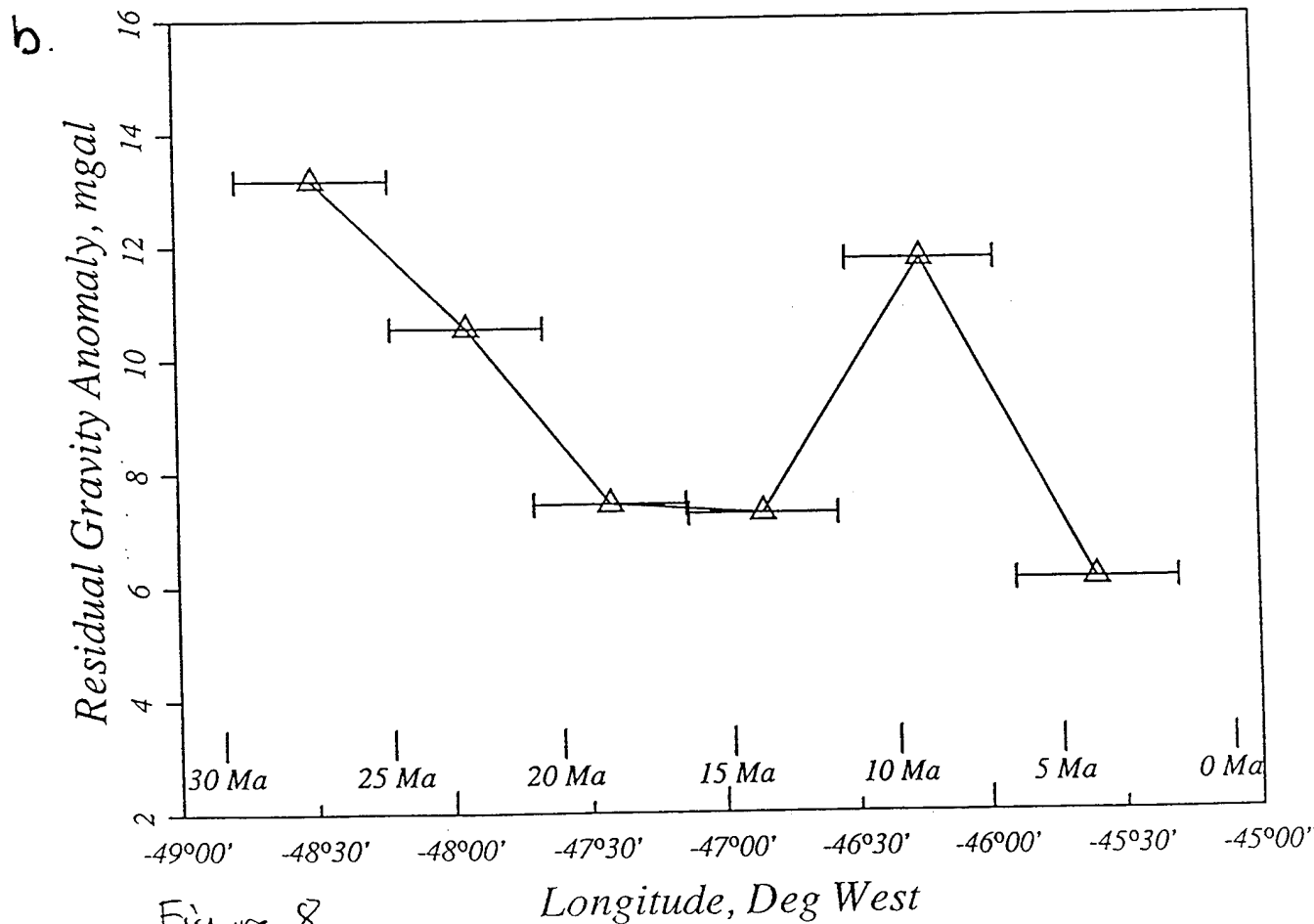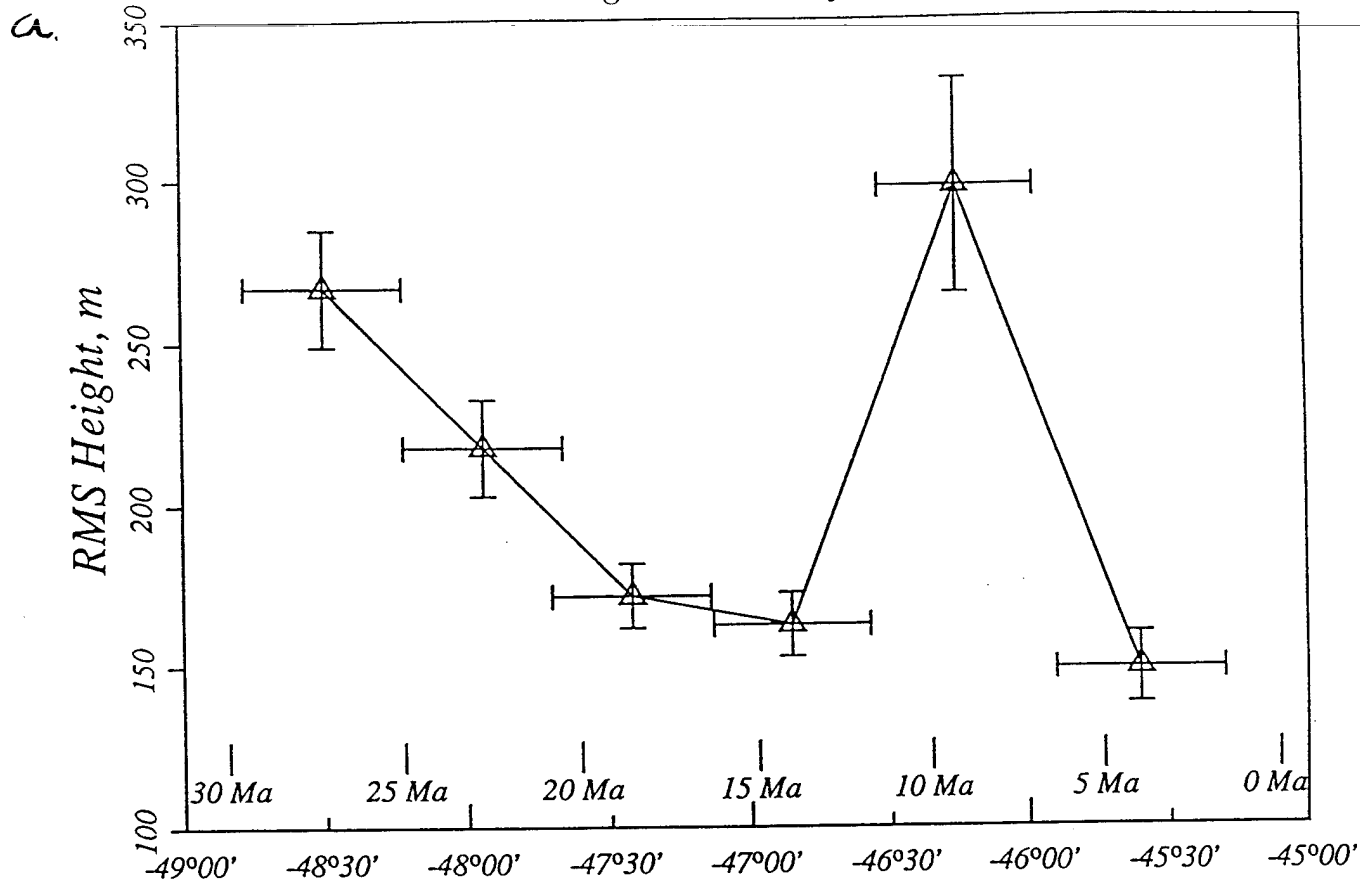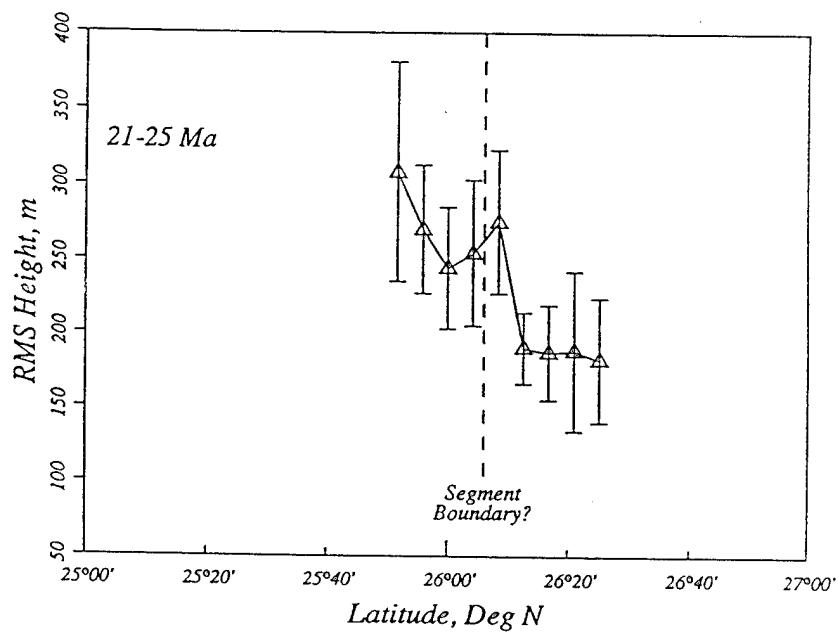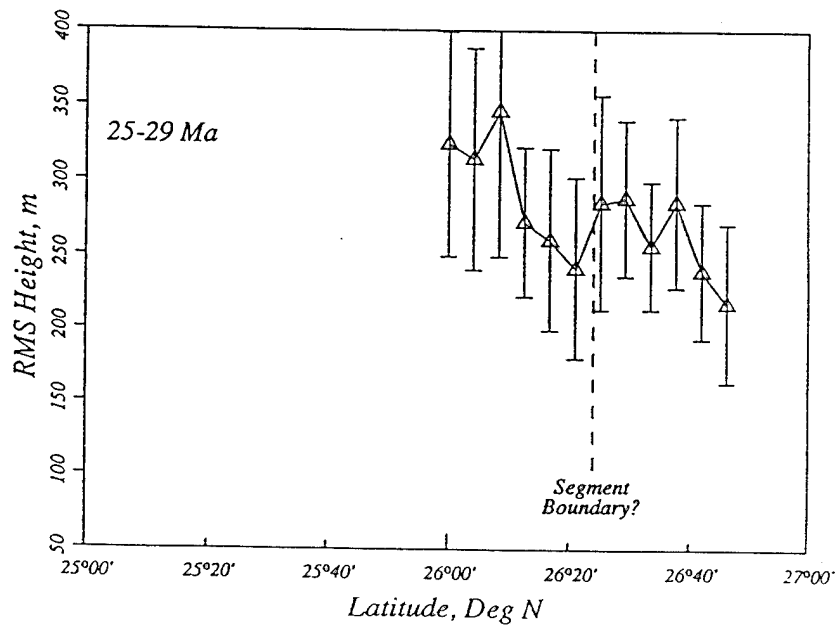
Figure 9

South Segment, 4-5 m.y. Averages

a.

b.

Figure 10

South Segment, 4-5 m.y. Averages

a.

b.

Figure 11